Stacking charts for converted waves in a transversely isotropic layer

Björn E. Rommel
Center for Wave Phenomena, Colorado School of Mines

ABSTRACT
Stacking charts are a convenient means for depicting shot and receiver points of a particular acquisition scheme. On them, one also sees, for example, that pairs of shots and receivers associated with any given common midpoint lie along straight, diagonally running lines. However, the stacking of a common-midpoint gather leads to reflection smear for mode-converted waves, even when the reflector is horizontal. The smearing problem is further altered when the medium is anisotropic and, especially, when the reflector dip is large. Instead, stacking of a common-reflection point (CRP) gather that collects shot-receiver pairs with rays illuminating the same reflection point on the reflector avoids reflection smear and improves the stacked signal.

Except for the conventional case of a pure-mode wave and a horizontal reflector, a CRP gather generally plots along a curve (henceforth, CRP curve) rather than a straight line on a stacking chart. Here, I discuss distortion and tilt of CRP curves for a single layer in the presence of transverse isotropy with a vertical symmetry axis and reflector dip. Also, I extend Frasier and Winterstein's straight-line approximation of a CRP curve, which holds for small offset-to-depth ratios, to transverse isotropy; however, such a straight-line approximation might fail even for modest offset-to-depth ratios.

As a consequence, the points representing actual shot-receiver pairs do not generally lie on any CRP curve, and binning is used to group all shot-receiver pairs with reflection points between the common-reflection points of neighboring CRP curves. To keep reflection smear within a CRP bin, binning should account for the actual distortion and tilt of CRP curves, especially when the offset is large. Then stacking would still be an appropriate method even in the presence of anisotropy. For a dipping reflector, however, only transformation to zero offset (TZO) or prestack migration can handle the shift of the zero-offset location due to dip. As the study demonstrates, however, those processes would also have to account for anisotropy. Unfortunately, all methods depend on detailed knowledge of the subsurface.

Key words: stacking chart, transverse isotropy, converted wave

Introduction

A stacking chart (Sheriff and Geldart, 1982) is a graphical representation of a 2D seismic acquisition scheme. The horizontal axis of the stacking chart denotes receiver position, and its vertical axis the source position. Hence, the locations of source and receiver for each seismic trace, characterized by a pair of source and receiver coordinates, are represented by a point on the stacking chart. Lines connecting source-receiver points associated with common-receiver, common-source, common-offset and common-midpoint gathers are straight along vertical, horizontal, 45° and 135° directions, respectively.

Each type of gather is defined by the locations of sources and receivers on the surface. For a reflected, pure-mode wave the common-midpoint gather happens to collect all pairs of source and receiver locations such that the specular rays illuminate the same reflection point on a ho-

rizontal reflector. Since the reflection point does not move laterally on the reflector for increasing offset-to-depth ratio, it can be considered the parameter of a common-midpoint gather. For a reflected, mode-converted wave or in the presence of a reflector dip, however, the lateral position of the reflection point does change with increasing offset-to-depth ratio. That change depends on the wavemodes for the downward and upward raypaths, the elastic properties of the medium, and the reflector dip. The rays collected by a common-midpoint gather do not focus on a single reflection point, thus, causing reflection-point smear and deterioration of the stack. Consequently, a common-reflection point (CRP) gather that explicitly accounts for the variable positioning of the reflection point, would be a better choice, although, in practice, we encounter problems specifying these variables especially for mode-converted waves (Rommel, 1994, 1995).

Since CRP and midpoint gathers do coincide for a pure-mode reflection from a horizontal reflector, the source and receiver positions for CRP gathers plot, in this case, along straight lines on the stacking chart. In general, however, we cannot expect such a behavior. In fact, the line depicting source and receiver positions for a CRP gather shows distortion and tilt. Henceforth, therefore, let's call this line a CRP line.

Despite this general behavior of any CRP curve, a CRP curve straightens if the horizontal distances between the shot and reflection point, on the one hand, and between the reflection and receiver point, on the other hand, are proportional to each other. This condition is always met by a reflected, pure-mode wave as long as the reflector is horizontal; also, it is met by mode-converted waves in the limit of large reflector depths or, precisely, of small offset-to-depth ratios (Frasier and Winterstein, 1990). In the following, assuming the same limit, I prove that this straightening also holds for a mode-converted wave in a transversely isotropic layer.

In reality, however, reflector depths are finite. In the following, I discuss the properties of reflection-point positions and, successively, the properties of the CRP curves for representative cases of transverse isotropy with a horizontal or mildly dipping reflector. As we will see, the quality of my straight-line approximation depends not only on the offset-to-depth ratio, but also on the elastic properties of the layer as well as on the reflector dip. In some cases, especially for dipping reflectors or in the presence of anisotropy, the CRP curve exhibits sizable curvature within typical offset-to-depth ratios.

CRP curves and CRP bins, which are strips between neighboring CRP curves, are of most interest for stacking. Stacking is a simple method to improve signal-to-noise ratio: the amplitudes of all traces with shot-receiver pairs having reflection points that lie inside a particular CRP bin are added. Sorting of traces into CRP bins is commonly based on straight lines on the stacking chart. However, as mentioned above, the straight-line approximation fails in the presence of anisotropy and, especially, of a reflector dip. Even for a horizontal reflector, sorting should account for the actual distortion and tilt of the CRP curves to keep reflection-point smear within the CRP bins. Then, if the moveout correction of traveltime also takes anisotropy into account (Hake, 1984; Rommel, 1993a), stacking is still an appropriate method to enhance signal-to-noise ratio, even in the presence of anisotropy. For a dipping reflector, transformation to zero-offset (TZO) (Rommel, 1996a,b,c) is more appropriate than stacking since only TZO accounts for the lateral shift of the reflection point (Deregowski and Rocca, 1981). However, TZO, too, has to consider the shift of the reflection point due to anisotropy demonstrated in this study.

Reflection Point Position

In this paper, I consider only a single layer. A ray travels from the source S to the reflector and back to the receiver R; it is reflected at the reflection point D on the reflector (see Figure A.1). The parameters that might influence the position of the reflection point D are, in general, the offset-to-depth ratio, the wavemodes, the elastic properties of the medium, and the reflector dip. In the following, I first discuss some properties of the reflection-point position with the intention of later gathering the rays illuminating the same reflection point on the reflector.

Consider vertical cross-sections such as in Figures 1 through 7, where the horizontal axis is the receiver offset and the vertical axis is the reflector depth. They illustrate the position of the reflection points with increasing reflector depth, where the wavemode and Thomsen's (1986) anisotropy coefficients are parameters.

The most simple case of a reflection is that of a pure-mode wave in an isotropic layer above a horizontal reflector (see Figure 1). As is well known, the reflection point is always located below the midpoint, that is the point midway between the source point and the receiver point. For increasing depth, the reflection points of a particular shot-receiver pair plot along the midline, that is the vertical line through the midpoint.

For a mode-converted wave in an isotropic medium above a horizontal reflector (see Figure 2), the reflection point moves laterally with increasing reflector depth. For a vanishingly small reflector depth, in fact, the reflection point is located at the receiver point. For increasing reflector depth and fixed offset, the reflection point approaches a vertical asymptote that crosses the surface

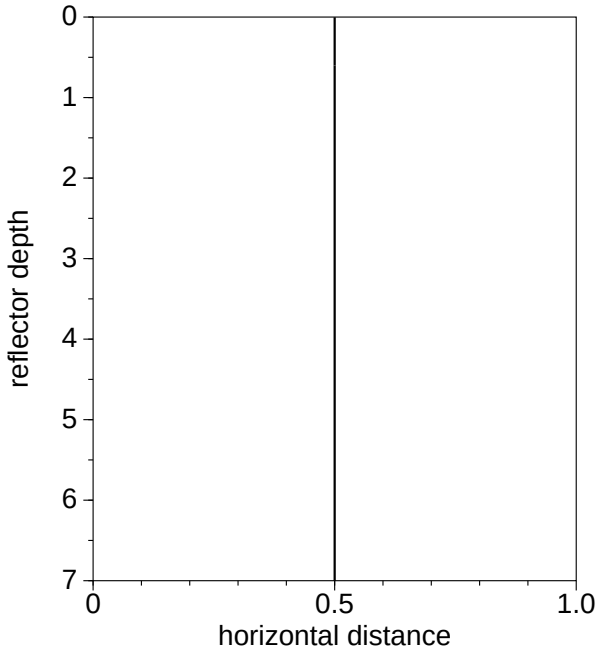

Figure 1. Reflection-point trajectory for a pure-mode wave in an isotropic layer above a horizontal reflector: Distances are measured relative to the offset between the source and the only receiver, but the axes are plotted at different scales. Here, the reflection points plot along the midline, a vertical line through the point halfway between the source point and the receiver point.

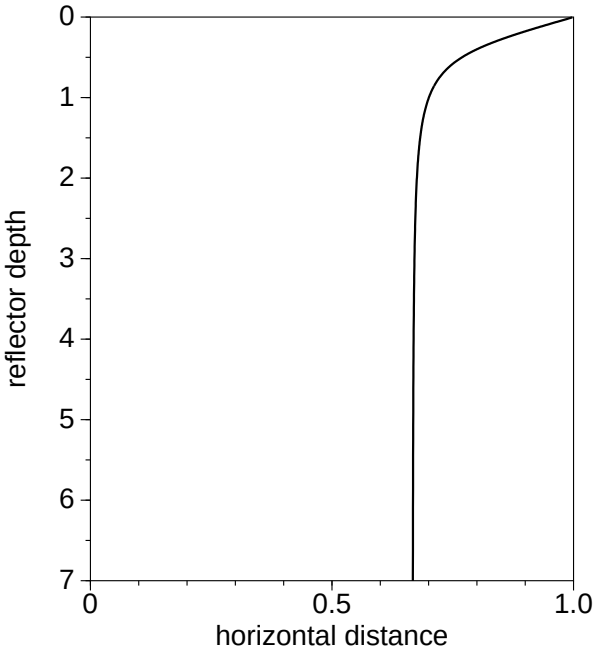

Figure 2. Reflection-point trajectory for a P-to-SV mode-converted wave in an isotropic layer above a horizontal reflector: For increasing reflector depth, the reflection point moves from the receiver point towards the source point and approaches a vertical asymptote that crosses the surface between the midpoint and the receiver point. Here, with a P- to SV-velocity ratio of 2, the lateral position of the asymptote is 2/3 times the offset. Compare with Figure 1 for the change in the position of the reflection points due to mode conversion.

not in the midpoint, but between the midpoint and the receiver point (Fromm et al., 1985).

The reflection-point trajectories of mode-converted waves in a single layer above a horizontal reflector also depend on the anisotropy (see Figures 3 and 4). First, consider positive anellipticity of 0.2 (in Figure 3), where anellipticity is here characterized by the difference of two of Thomsen's (1986) anisotropy coefficients $\epsilon - \delta$. The reflection point again starts out at the receiver point and, for increasing reflector depth, moves laterally towards the source point, but it moves much further towards the source point than it does in an isotropic layer (compare with Figure 2). Again, the reflection-point trajectories approach vertical asymptotes. Depending on the particular choice of anisotropy coefficients, the asymptotes might cross the surface between the source point and the midpoint. Recall, that the reflection point of the pure-mode wave is always located beneath the midpoint; hence, in contrast to an isotropic medium, the reflection point of the P-to-SV mode-converted wave might be on either side of the reflection point of the pure-mode wave (Rommel, 1995). For a SV-to-P mode-converted wave, the trajectories have mirror symmetry about the midline to those shown here.

In a medium having negative anellipticity, the reflection point, again, starts out at the receiver point and moves towards the source point, but it does so much less than in an isotropic medium (compare with Figure 2). For strong negative anellipticity, such that a triplication in the SV-wavefront occurs near the vertical direction, the reflection point turns back and approaches a vertical asymptote that crosses the surface beyond the receiver point (see Figure 4). For less negative anellipticity, the asymptote still crosses the surface between the asymptote for an isotropic medium and the receiver point (Rommel, 1995).

For a dipping reflector, the dependence of the reflection point trajectories on the anisotropy is overwhelmed by the dependence on the reflector dip itself (see Figures 5 through 7). Hence, in the following, I discuss only the case of a vertical symmetry axis, not of a symmetry axis perpendicular to the reflector. The reflection point of a pure-mode wave starts out at the source point, no longer at the midpoint, then moves towards the receiver point, and arcs back to approach an asymptote that is perpendicular to the reflector for an isotropic medium

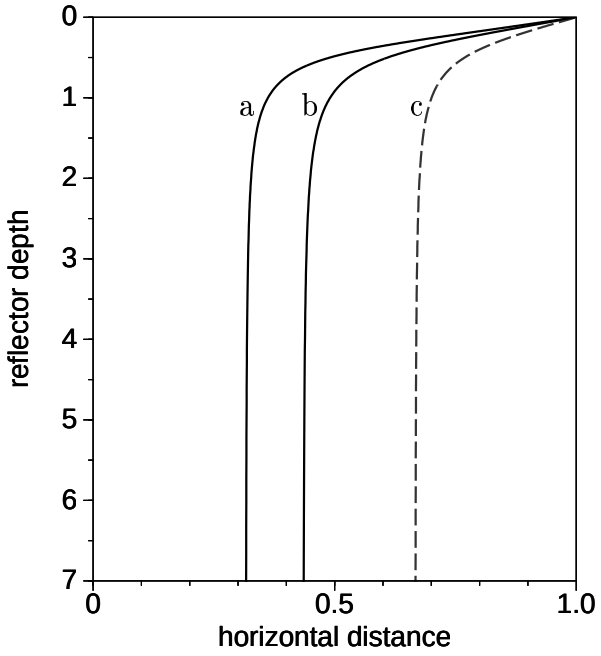

Figure 3. Reflection-point trajectories for P-to-SV mode-converted waves in a layer having positive anellipticity above a horizontal reflector: The medium is transversely isotropic with a vertical symmetry axis. The vertical velocities are as in Figure 2. Thomsen's (1986) anisotropy coefficients are, in case (a), $\delta = -0.2$ and $\epsilon = 0.0$ and, in case (b), $\delta = 0.0$ and $\epsilon = 0.2$. The anellipticity, $\epsilon - \delta$, is positive with 0.2 in both cases. For comparison, in case (c), the layer is isotropic as in Figure 2. With increasing reflector depth, the reflection point moves from the receiver point towards the source point, more so than in the isotropic medium of case (c), and approaches an asymptote. Here, the asymptotes are even between the source point and the midpoint, at 0.32 and 0.43 times the offset for the cases (a) and (b), respectively.

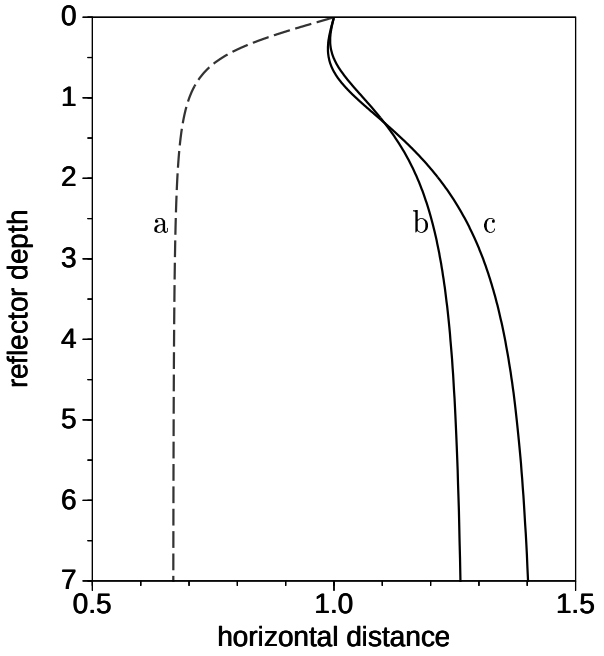

Figure 4. Reflection-point trajectories for P-to-SV mode-converted waves in a layer having negative anellipticity above a horizontal reflector: The horizontal axis is shifted by 0.5. The medium is transversely isotropic with a vertical symmetry axis. The vertical velocities are as in Figure 2. Thomsen's (1986) anisotropy coefficients are, in case (b), $\delta = 0.2$ and $\epsilon = 0.0$ and, in case (c), $\delta = 0.0$ and $\epsilon = -0.2$. The anellipticity, $\epsilon - \delta$, is thus negative with -0.2 in both cases. For comparison, in case (a), the medium is isotropic as in Figure 2. With increasing reflector depth, the reflection point moves only slightly from the receiver point towards the source point, then turns back, and approaches an asymptote. Here, the asymptotes are even beyond the receiver point, at 1.27 and 1.43 times the offset for the cases (b) and (c), respectively. Also, note, that the asymptotes are approached much more slowly than those in Figure 3.

(see Figure 5). The reflection point of a mode-converted wave starts out at some nonzero depth between the source point and the receiver point and turns into an inclined asymptote (see Figure 6). The reflection-point trajectories of mode-converted waves in an anisotropic medium differ mainly in the inclination of the asymptote; also, for increasing anellipticity, the top point of the reflection-point trajectories move towards the receiver point and to slightly larger depths (see Figure 7).

In all cases discussed above, the reflection points approach asymptotes for increasing reflector depth. This property will become the basis for an asymptotic approximation of the CRP curve that, strictly speaking, holds only in the limit of small offset-to-depth ratios. Thus, since the reflection points approach the asymptote smoothly, the asymptotic approximation of the CRP curve becomes progressevily more accurate with increasing reflector depth.

Graphical Representation of CRP Gathers in Stacking Charts

As seen above, the relationship between the horizontal distances from the shot x_S to the reflection point x_D, on the one hand, and from the shot x_S to the receiver point x_R, on the other hand, can be highly non-linear. For a small offset-to-depth ratio, however, Snell's law and, consequently, the relationship between these two distances can be linearized; in the limit of vanishing offset-to-depth ratio the two distances become proportional (see Appendix A):

$$x_D - x_S = \frac{k}{k-1}\,(x_R - x_S)\,, \qquad (1)$$

where x_D, x_S, and x_R are the lateral positions of the reflection, source and receiver point, respectively, and k

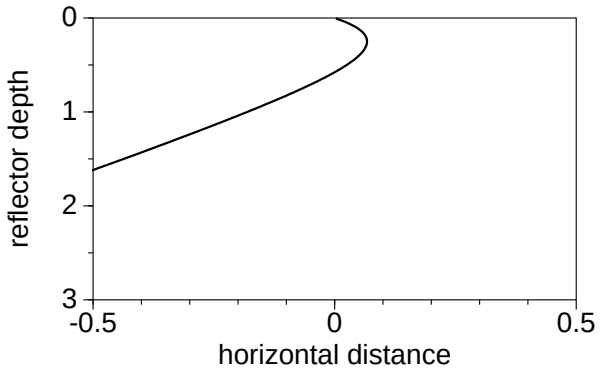

Figure 5. Reflection-point trajectory for a pure-mode wave in an isotropic layer above a reflector with 30° dip: The horizontal axis is shifted by -0.5. With increasing reflector depth, the reflection point moves from the source point towards the midpoint, but turns back, and approaches an inclined asymptote. Compare with Figure 1 for a non-dipping reflector.

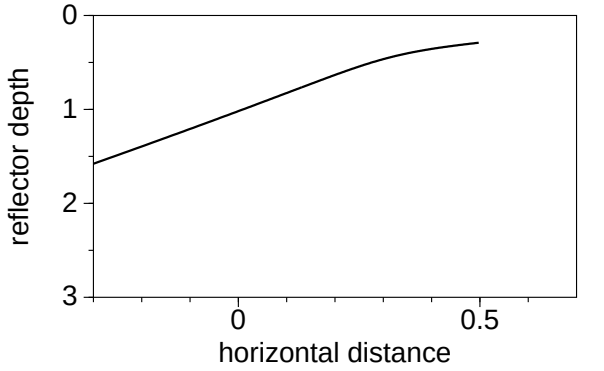

Figure 6. Reflection-point trajectory for a P-to-SV mode-converted wave in an isotropic layer above a reflector with 30° dip: The horizontal axis is shifted by -0.3. The vertical velocities are as in Figure 2. The trajectory tops at a certain depth between the source point and the receiver point. With increasing reflector depth, the reflection point approaches an inclined asymptote. Compare with Figure 2 for a non-dipping reflector.

is an yet unknown constant factor that, as we will see, depends on the elastic properties of the medium and the reflector dip. Rearranging (1) gives the linear relationship between source and receiver points, for fixed reflection points, on the stacking chart

$$x_S \quad = \quad k x_R + (1-k)\, x_D, \tag{2}$$

where the constant factor k denotes the slope of the line.

As is well known, a reflected, pure-mode wave above an horizontal reflector gives rise to a straight line on the stacking chart, because the raypaths are symmetric with respect to the common-depth point. Also, these lines pass diagonally through the stacking chart, as

$$k \quad = \quad -1 \tag{3}$$

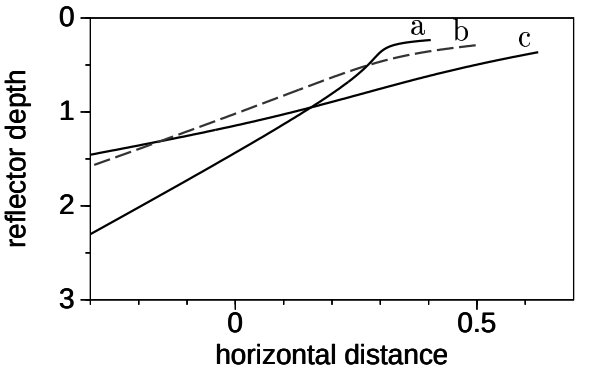

Figure 7. Reflection-point trajectory for P-to-SV mode-converted waves in a strongly anisotropic layer above a reflector with 30° dip: The horizontal axis is shifted by -0.3. The medium is transversely isotropic with a vertical symmetry axis. The vertical velocities are as in Figure 2. Thomsen's (1986) anisotropy coefficients are, in case (a), $\delta = 0.2$ and $\epsilon = 0.0$, and, in case (c), $\delta = 0.0$ and $\epsilon = 0.2$, thus showing negative and positive anellipticity, respectively, with the same absolute value of 0.2. For comparison, in case (b), the medium is isotropic. As in Figure 6, the trajectories top at certain depths between the source point and the receiver point. For increasing anellipticity, the top point shifts towards the receiver point and a slightly larger depth. With increasing reflector depth, for each case, the reflection point moves towards and continues beyond the source point, approaching an inclined asymptote. The inclination of the asymptotes depends on the elastic properties of the medium; it generally decreases with increasing anellipticity. Compare with Figures 3 and 4 for a non-dipping reflector.

for this case.

This symmetry is broken, however, for a reflected, mode-converted wave; the reflection point is governed by a complicated fourth-order polynomial in offset and reflector dip (Tessmer and Behle, 1988). Nevertheless, condition (1) is met in the limit of a small offset-to-depth ratio (Fromm et al., 1985). Consequently, the CRP curves are still straight for small offset-to-depth ratios (Frasier and Winterstein, 1990). The slope, in the limit, however, depends on the elastic properties of the medium:

$$k \quad = \quad -\frac{v_p}{v_s}, \tag{4}$$

where v_p and v_s are the P- and SV-phase velocities, and I assumed throughout that the downgoing wave is the P-wave.

Transverse isotropy does not alter the symmetry of the reflected, pure-mode wave, provided that the symmetry axis is vertical (as in a so-called VTI medium). Transverse isotropy, however, does shift the reflection point of a reflected, mode-converted wave for given source and receiver positions (Eaton, 1991). Nevertheless, in the limit of small offset-to-depth ratios, condition

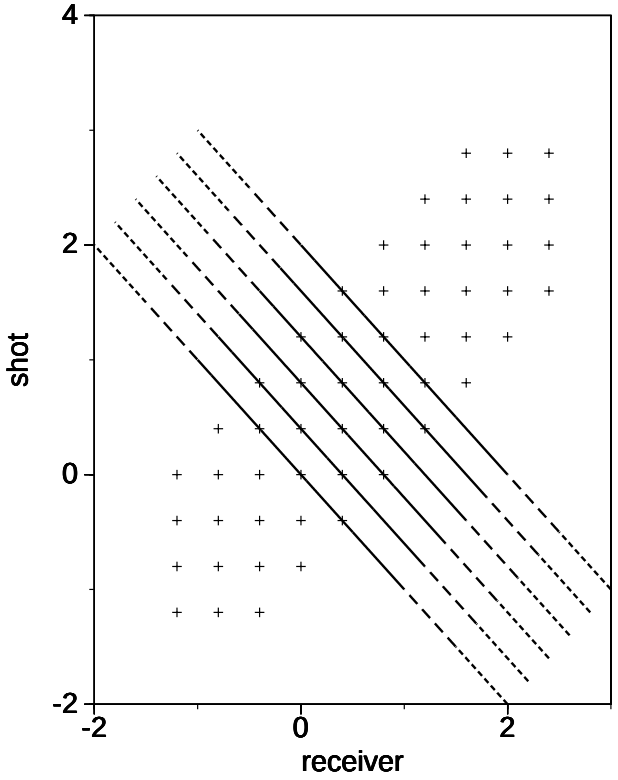

Figure 8. CRP curves for a pure-mode wave in an isotropic medium above a horizontal reflector: Receiver and shot positions are scaled by the reflector depth. The solid lines represent the parts of a CRP curve with an absolute shot-receiver offset between 0.0 and 1.0 times the reflector depth, the long dashes the parts between 1.0 and 1.5 times the reflector depth, and the short dashes the parts between 1.5 and 2.0 times the reflector depth. The crosses mark shot and receiver locations of a hypothetic (sparse) acquisition. Here, the medium is isotropic, and the reflector is horizontal. In this case, the CRP curves are straight and cross diagonally through the stacking chart.

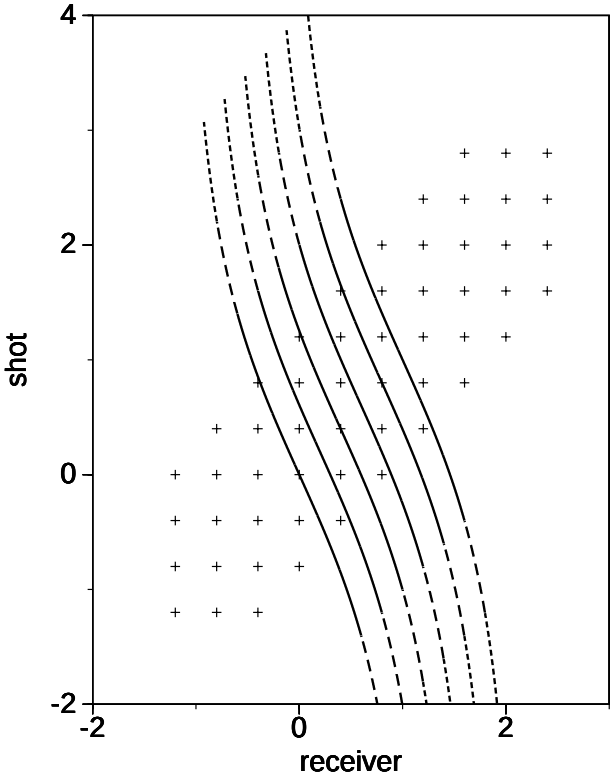

Figure 9. CRP curves for a P-to-SV mode-converted wave in an isotropic medium above a horizontal reflector: Due to mode conversion, the CRP curves are no longer straight, but curved in the form of an "S" (compare with Figure 8 for a pure-mode wave), with varying slope that is generally larger than the slope of a pure-mode wave. Here, and in Figures 10 through 13 and 15 through 17, the P- to SV-wave velocity ratio is 2. Note that the straight-line approximation is reasonably accurate only in the center, where offset-to-depth ratio is small.

(1) is met again, and the slope becomes (see A.26)

$$k = -\frac{v_{p0}}{v_{s0}} \frac{[1+2\delta]}{\left[1+2\frac{{v_{p0}}^2}{{v_{s0}}^2}(\epsilon-\delta)\right]}, \quad (5)$$

where v_{p0} and v_{s0} denote the P- and SV-phase velocity, respectively, in the vertical direction, and δ and ϵ are Thomsen's (1986) anisotropy coefficients.

Generally, for any mode-converted wave, the slope k of a CRP curve depends on the elastic properties of the medium. Again, these expressions for the slope hold only in the limit of a vanishing offset-to-depth ratio; generally, however, an exactly computed CRP curve deviates from a straight line with the deviation depending on the offset-to-depth ratio as well as on the elastic properties, as discussed in the next section.

Stacking Charts

Horizontal reflector

Pure-mode wave in an isotropic layer

For a pure-mode wave in an isotropic layer, the raypaths of the downgoing and upgoing waves are symmetric with respect to the reflector normal. If the reflector is horizontal, that is parallel to the surface, shot and receiver points are located symmetrically on either side of the reflection point, regardless of the actual shot-receiver distance. That is why CRP curves plot along straight lines with a slope of 45° (Figure 8). Lines of successive CRP curves are thus parallel to each other. Also, with a common-reflection spacing of half the receiver spacing, each shot-receiver pair plots as a point on one of the CRP curves.

Also, since the reflection point is always below the midpoint in this situation, a common-midpoint gather

coincides with a common-reflection point gather. This coincidence no longer holds for either a mode-converted wave or in the presence of a reflector dip.

Pure-mode wave in an anisotropic layer

Even in a transversely isotropic layer with a vertical symmetry axis, the raypaths of the downgoing and upgoing waves remain symmetric with respect to the reflector normal. Hence, the CRP curves are still straight lines. However, a SV-wavefront can show a triplication. Then, the same reflection point can be illuminated by different branches of the wavefront; hence, it might be illuminated by the rays of as many as three different shot-receiver pairs. Although the CRP curve remains straight, it actually consists (in parts) of three different straight lines.

Mode-converted wave in an isotropic layer

Due to mode conversion, the raypaths of the downgoing and upgoing waves are no longer symmetric with respect to the reflector normal. In the limit of vanishing reflector depth, in fact, the reflection point is located at the receiver (assuming that the downgoing wave is a P-wave, and the recorded wave is an SV-wave). For increasing depth, the reflection point approaches a vertical asymptote that crosses the surface somewhere between the midpoint and the receiver point (Fromm et al., 1985), again assuming a P-to-SV mode-converted wave.

For very large reflector depths and, hence, small ray angles of the downgoing and upgoing waves, their relationship as expressed by Snell's law can be linearized. Then, the horizontal distances between the shot and reflection point, on the one hand, and between the receiver and reflection point, on the other hand, become proportional. Consequently, the CRP curve can be approximated by a straight line, where the slope of the CRP curve equals the negative P- to SV-wave velocity ratio (Frasier and Winterstein, 1990). However, as exemplified in Figure 9, the straight-line approximation fails for large offset-to-depth ratios, where the assumption of a linear relationship between the ray angles does not hold. Generally, the larger the velocity ratio the smaller the offset-to-depth ratio where the straight-line approximation holds with the same accuracy.

Even in the straight-line approximation, reflection points of rays from all shot-receiver pairs lie on uniformly spaced lines only if the ratio of the P-wave to the SV-wave velocity is an integer number (Eaton, 1991). Hence, in general, we have to sort the shot-receiver pairs into CRP bins rather than CRP lines when forming CRP gathers, thus accepting some reflection smear. More precisely speaking, a CRP bin includes all shot-receiver pairs with reflection points on the reflector within a strip

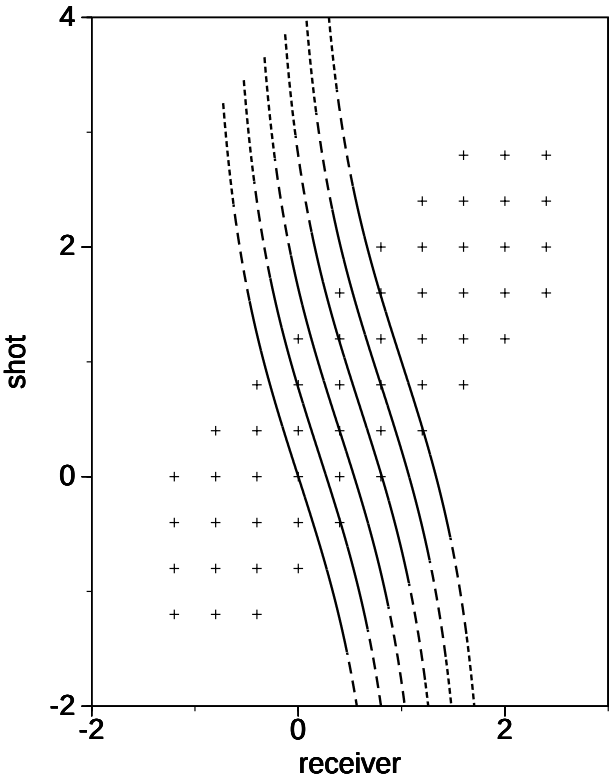

Figure 10. CRP curves for a P-to-SV mode-converted wave in an elliptically anisotropic medium above a horizontal reflector: The medium has anisotropy coefficients $\epsilon = 0.2$ and $\delta = 0.2$. The CRP curves show similiar distortion to that for an isotropic medium (compare with Figure 9), but are slightly steeper.

with fixed width, for example, of a quarter the receiver group interval on either side of the CRP line. Moreover, the number of shot-receiver pairs per bin varies periodically, here between 4 and 2 per bin (see Figure 9). This requires amplitude balancing between bins, especially if the fold is low (Eaton, 1991; Eaton and Lawton, 1992). Both problems – the necessity of binning and amplitude balancing – will be even more pronounced in the presence of anisotropy or a reflector dip.

Here, for a ratio of the P-phase velocity and SV-phase velocity of 2, the slope in the center of Figure 9 is -2 (see equation 4). For large offset-to-depth ratios, the CRP curve begins to resemble an "S", and the straight-line approximation fails.

Mode-converted wave in an elliptically anisotropic layer

In an elliptically anisotropic medium the form of the P-wavefront is elliptic, but that of the SV-wavefront is still spherical. Since I also assume a vertical symmetry axis of the anisotropy, the raypath of a pure-mode wave is still symmetric. Therefore a CRP curve is still a straight line,

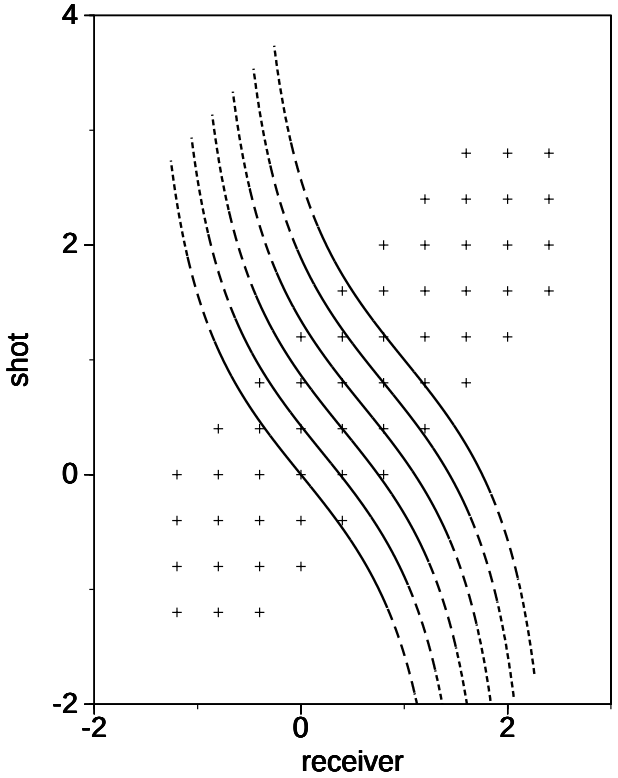

Figure 11. CRP curves for a P-to-SV mode-converted wave in an anisotropic medium above a horizontal reflector: The medium has a small positive anisotropy coefficient $\epsilon = 0.1$, while $\delta = 0.0$. The CRP curves are more distorted and slightly more tilted than are those for an isotropic medium (compare with Figure 9). Also, compare with the CRP curves for a negative δ (in Figure 12), but with the same value $\epsilon - \delta = 0.1$.

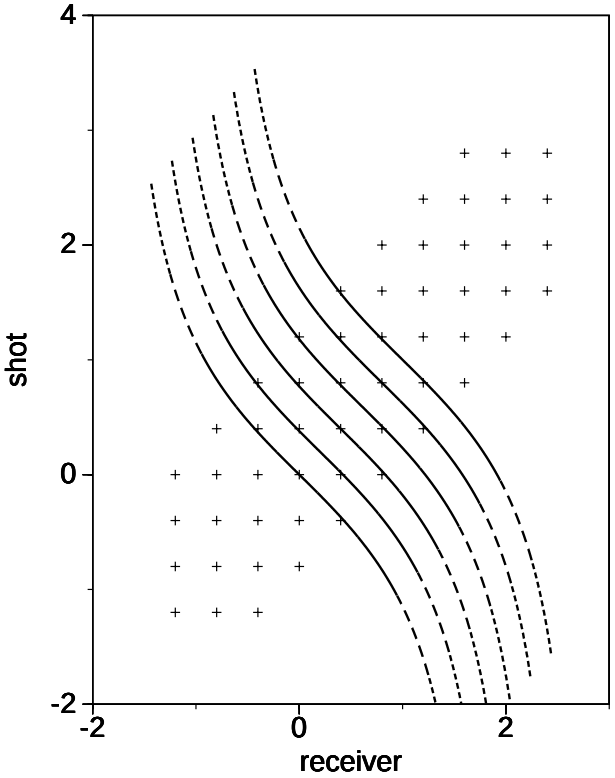

Figure 12. CRP curves for a P-to-SV mode-converted wave in an anisotropic medium above a horizontal reflector: The medium differs from that for Figure 11 in that it has a small negative anisotropy coefficient $\delta = -0.1$, while $\epsilon = 0.0$. The CRP curves are similiar to those for an anisotropic medium with a small positive value of ϵ, but with the same value $\epsilon - \delta = 0.1$ (see Figure 11).

no matter how the wave velocity changes with the ray angle (not shown here). However, mode conversion again breaks the symmetry: since the velocity of the downgoing P-wave changes with direction, the reflection angle of the upgoing SV-wave also changes. Consequently, the CRP curve does show some influence of elliptical anisotropy.

For positive values of Thomsen's (1986) anisotropy coefficients $\epsilon = \delta$, the CRP curves are slightly more tilted than those in an isotropic medium (see equation 5), but have comparable curvature (compare Figure 10 with Figure 9). Here, in Figure 10 the slope in the center is -2.8

The straight-line approximation is as accurate as for an isotropic layer, failing as before for large offset-to-depth ratios. Generally, the larger the ratio of the P-phase velocity and SV-phase velocity in the vertical direction, and the larger the ellipticity $\epsilon = \delta$, the smaller the offset-to-depth ratio at which accuracy of the straight-line approximation is maintained.

Mode-converted wave in layers with constant anellipticity

Above, we saw that the distortion of the CRP curves is nearly independent of the anisotropy for an elliptically anisotropic medium. Here, I consider layers with constant anellipticity, characterized by the difference of the anisotropy parameters $\epsilon - \delta$, but with different combinations of ϵ and δ. In a transversely isotropic medium, not only the P-wave velocity, but also the SV-wave velocity depends on the phase angle.

For a small positive value of ϵ, with $\delta = 0$, the curvature is stronger than that for an isotropic medium (Figure 11). On the other hand, a small negative value of δ and $\epsilon = 0$, such that $\epsilon - \delta$ is unchanged, causes nearly the same distortion and tilt of the curves (Figure 12). The slopes in the center are similiar with 1.1 and 0.9, respectively (see equation 5). This indicates a primary dependence on the anellipticity $\epsilon - \delta$.

Generally, for the same ratio of P- and SV-phase velocity in the vertical direction, the larger the anellipticity

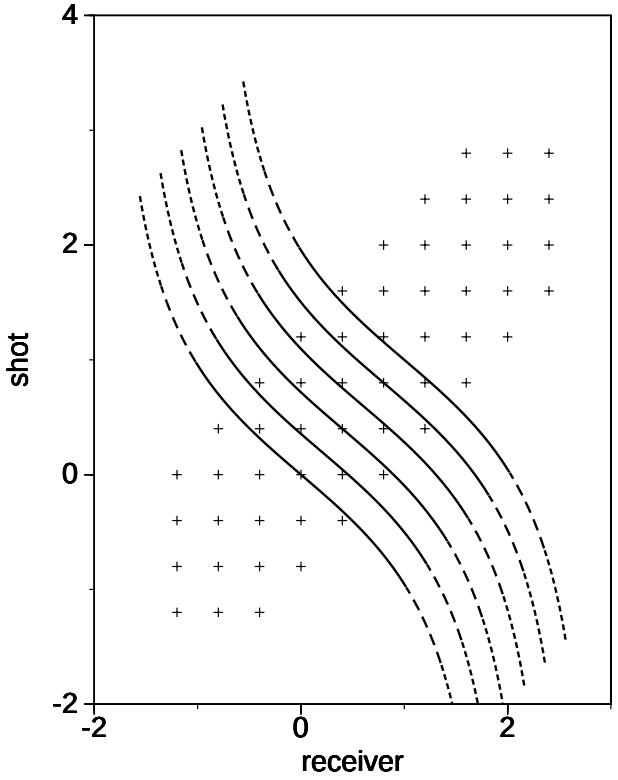

Figure 13. CRP curves for a P-to-SV mode-converted wave in a strongly anisotropic medium above a horizontal reflector: The medium has a large positive anisotropy coefficient $\epsilon = 0.2$, while $\delta = 0.0$. The CRP curves are generally less tilted than those for a smaller value of ϵ and, hence, smaller anellipticity (see Figure 11).

$\epsilon - \delta$, the smaller the offset-to-depth ratio at which the straight-line approximation fails. However, the dependence on the specific combination of the anisotropy parameters δ and ϵ is negligible.

Mode-converted wave with a triplication

For large positive values of $\epsilon - \delta$, the SV-wavefront shows a triplication at large ray angles for large ray angles frm the vertical direction. However, ray angles of the upgoing SV-wave that are so large that a triplication in the reflected SV-wave actually arises are hardly realized in practice. Such a situation requires a nearly horizontal incidence of the downgoing P-wave and a small ratio of the P- and SV-phase velocity. Hence, triplication can influence the CRP curves only at very large offset-to-depth ratios. Here, for example, we don't observe the influence of a triplication in the reflected SV-wavefront (Figure 13). Nevertheless, the large positive anellipticity does cause a strong distortion of the CRP curves for large offset-to-depth ratios. The situation changes dramatically, if the reflector dip is so large that the reflected rays do form a triplication in the upgoing SV-wave (see below and Figure 17).

Dipping reflector

pure-mode wave in an isotropic layer

The more a reflector dips, the more up-dip the reflection point moves and the more dependent is that point on source-receiver offset. The reflection points are no longer equally spaced. For decreasing reflector depth, the reflection points move towards the source point for a positive reflector dip (see Figure 1), but towards the receiver point for a negative reflector dip. Hence, the CRP curves arc strongly and in a concave upward form (Figure 14); for very large offset-to-depth ratios, the CRP curves become nearly horizontal in the down-dip direction, but nearly vertical in the up-dip direction (lower right and upper left corner of Figure 8). Clearly, they are no longer straight as for a horizontal reflector (see Figure 8). As a consequence, the straight-line assumption is unacceptable for all offset-to-depth ratios.

Mode-converted wave in an isotropic layer

As for the reflected, pure-mode wave the CRP curves for the mode-converted wave arc in a concave upwards form (Figure 15). Interestingly, the curving is less severe for the mode-converted wave than for the pure-mode wave (Figure 14). This is because mode conversion causes convex upward curvature, while dip introduces concave upward curvature for large offsets in the down-dip direction (here, in the lower right corner of the figures); thus, they have opposite action.

Mode-converted wave in an elliptically anisotropic layer

As for the case with a horizontal reflector, ellipticity increases the slope, but hardly alters the curvature (compare Figure 16 with Figure 15). Again, the dependence of the CRP curves on the ellipticity $\delta = \epsilon$ is small; the actions of the two anisotropy parameters δ and ϵ roughly counteract one another.

Mode-converted wave with a triplication

As seen above, anellipticity changes the curvature of the CRP curves. An extreme case is a triplication in the upgoing SV-wave for large ray angles from the vertical direction. For a horizontal reflector, rays belonging to such a triplication can be observed only at extremely large offset-to-depth ratio, if at all (see Figure 13). A dipping reflector, however, allows the triplication to show up even for realistic offset-to-depth ratios (Figure 17). Then, a receiver might record a wave at three different times. The

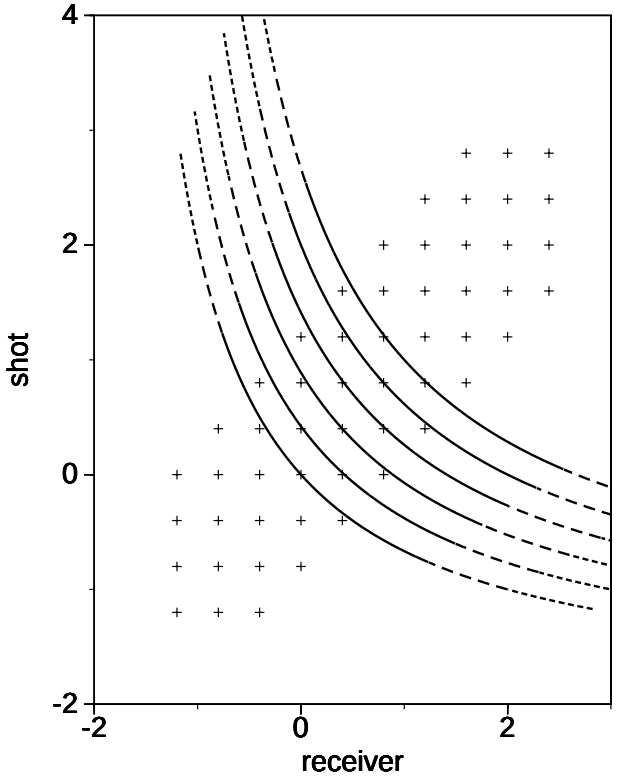

Figure 14. CRP curves for a pure-mode wave in an isotropic medium above a reflector with 30° dip: Due to the reflector dip, the CRP curves are no longer straight, but show a strong concave upward curvature (compare with Figure 8).

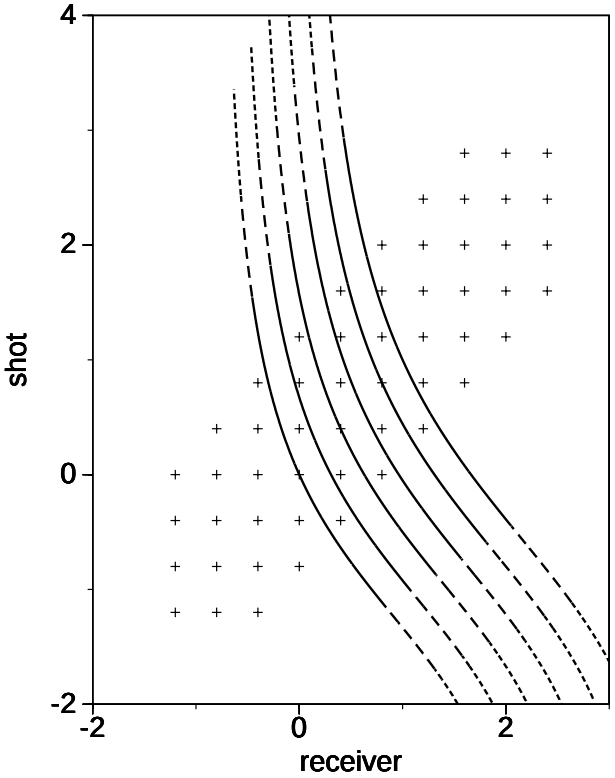

Figure 15. CRP curves for a P-to-SV mode-converted wave in an isotropic medium above a reflector with 30° dip: Due to the reflector dip, the "S"-shaped curvature of the CRP curves in Figure 9 has changed to a concave upward curvature.

corresponding raypaths and, hence, the reflection points of these events, of course, are different. Alternatively, one can say that a receiver might record up to three waves that are generated at different source points, but illuminate the same reflection point. Consequently, the CRP curves are predominately vertical.

Conclusions

Stacking charts are a simple, commonly-used graphical tool to illustrate coverage of common-reflection points for particular acquisition schemes. Here, I discussed stacking charts for a single layer with transverse isotropy and above a dipping reflector.

For a single layer above a horizontal reflector, CRP curves of a reflected, pure-mode wave plot along straight lines, and those of a reflected, mode-converted wave still plot along approximately straight lines on the stacking chart. While anisotropy does not influence the CRP curves of a pure-mode wave, it increases the distortion and changes the tilt of the CRP curves of a mode-converted wave. However, the anisotropy is overwhelmed by the reflector dip. Generally, in the presence of a reflector dip, the CRP curves of a pure-mode wave is even more distorted that those of a mode-converted wave. Also, due to the reflector dip, a triplication that occurs in the wavefront of the upgoing SV-wave in a medium with large positive anellipticity becomes observable; in this case, the CRP curves are predominately vertical. A straight-line approximation would fail even for modest offset-to-depth ratios.

The straight-line assumption is, in fact, based on a linear relationship between the distances traveled by the downgoing and upgoing waves. Even for a mode-converted wave in an isotropic medium, this assumption fails for large offset-to-depth ratios, the larger the velocity contrast the smaller the offset-to-depth ratio where the assumption breaks down. For an anisotropic medium or a dipping reflector, a linear relationship still exists in the limit of small offset-to-depth ratios, but the velocity variation due to anisotropy or the reflection point smear due to reflector dip causes the linear relationship to fail even within small, commonly used offset-to-depth ratios.

This study demonstrates that anisotropy and, especially, reflector dip increase the distortion and change the tilt of CRP curves. To keep reflection-point smear within the CRP bins, stacking should take anisotropy

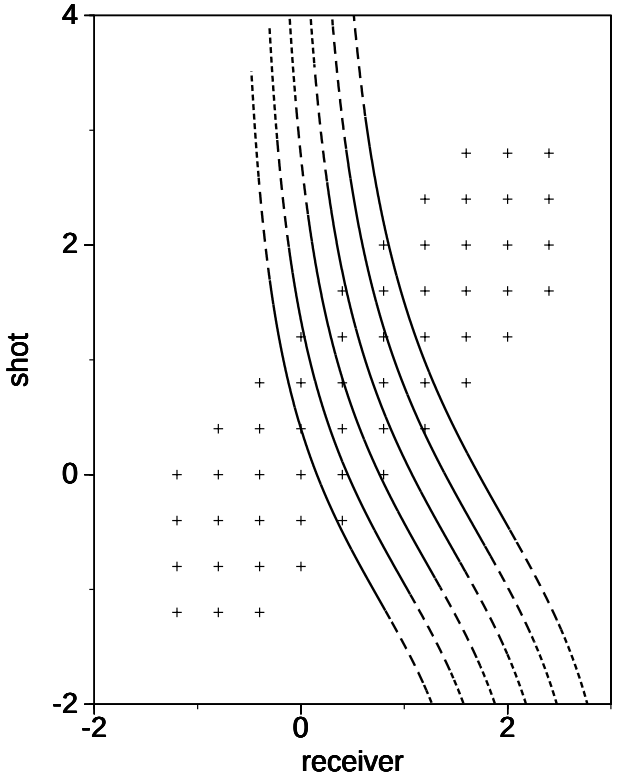

Figure 16. CRP curves for a P-to-SV mode-converted wave in an elliptically anisotropic medium above a reflector of 30° dip: The anisotropy coefficients are as in Figure 10. Compared with the CRP curves for an isotropic medium (Figure 15) the slope of the CRP curves is somewhat larger, but the curvature is about the same.

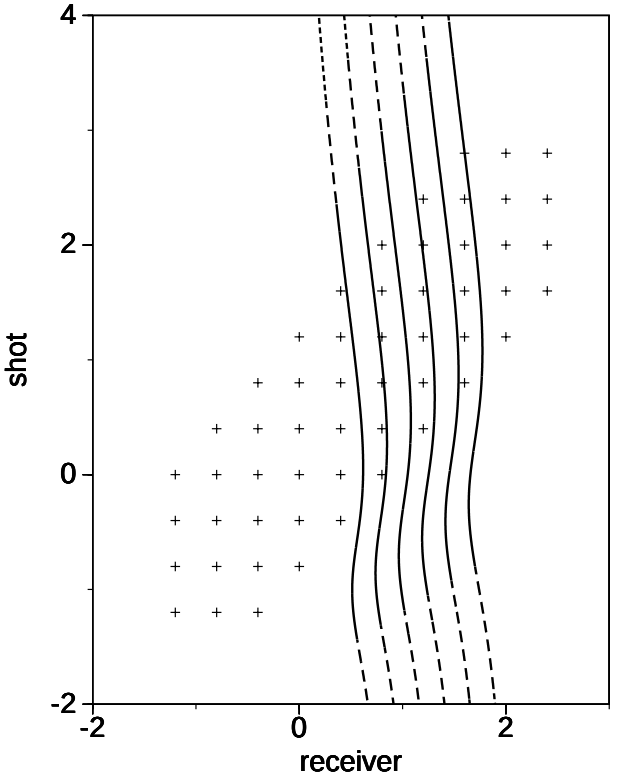

Figure 17. CRP curves for a P-to-SV mode-converted wave in a strongly anisotropic medium above a reflector with 30° dip: The anisotropy coefficients are as in Figure 13. The slope is nearly vertical, and receivers are crossed up to three times. Due to the reflector dip, rays within the triplication are recorded (in contrast to the situation in Figure 13).

and reflector dip into account. In the presence of a reflector dip, however, transformation to zero offset (TZO) would be a superior, though more costly alternative since it also accounts for the shift of the reflection point due to reflector dip. Since anisotropy further alters the distortion of CRP curves already caused by the reflector dip, TZO, too, should take anisotropy into account. Unfortunately, all methods require knowledge of the anisotropy in advance.

References

Eaton, D. W. S., 1991, Seismic migration/inversion for transversely isotropic elastic media: Ph.D thesis, The University of Calgary.

Eaton, D. W. S., Lawton, D. C., 1992, Short Note: P-SV stacking charts and binning periodicity: Geophysics, **57**, 745-748.

Frasier, C., Winterstein, D., 1990, Analysis of conventional and converted mode reflections at Putah sink, California using three-component data: Geophysics, **55**, 646-659.

Fromm, G., Krey, T., and Wiest, B., 1985, Static and dynamic corrections, *in*, Dohr, G., Ed., Seismic shear waves: Handbook of geophysical exploration, Geophys. Press, Vol. 15a, 191-225.

Hake, H., Helbig, K., and Mesdag, C. S., 1984, Three-Term Taylor Series for $t^2 - x^2$-Curves of P- and S-Waves over Layered Transversely Isotropic Ground: Geophysical Prospecting, **32**, 828-850.

Rommel, B. E. 1996c, Kinematic TZO-response curves: an iterative approach for mode conversion and transverse isotropy: 56th Ann. Internat. Mtg., Soc. Expl. Geophys., Expanded Abstracts, 1559–1562.

Rommel, B. E., 1996b, Dip Moveout Processing (DMO) for Converted Waves in Transversely Isotropic Media: 58th Mtg., Europ. Assn. Geoscient. Eng., No. P136.

Rommel, B. E., 1996a, TZO Response Curves: an Iterative Approach for Mode Conversion and Transverse Isotropy: Tech. rept. CWP 203, Center for Wave Phenomena, Colorado School of Mines.

Rommel, B. E., 1995b, Laufzeitanalyse von reflektierten/konvertierten Wellen in geschichteten Medien bei schwach transversaler Isotropie (Traveltime analysis

of reflected/converted waves in layered media with weak transverse isotropy), *in* Teßmer, G. [Edt.], Lithologieerkundung für den Tiefenaufschluß mit seismischen Methoden (LITASEIS): Refraktionsseismik, Bohrlochmessungen und Anisotropieuntersuchungen (Lithology determination with seismic methods at large depths (LITASEIS): refraction seismics, borehole measurements, and anisotropy analysis), DGMK 397-2/2, Deutsche Wissenschaftliche Gesellschaft für Erdöl, Erdgas und Kohle; BMFT 0326812E2 (LITASEIS), Bundesminister für Forschung und Technologie.

Rommel, B. E., 1995a, Accuracy of Anisotropic Layer Parameters Estimated by Traveltime Analysis: 57th Mtg., Europ. Assn. Expl. Geophys., Extended Abstracts, No. P023.

Rommel, B. E., 1994, Traveltime Analysis for Weak Anisotropy - Estimation of Layer Parameters: 56th Mtg., Europ. Assn. Expl. Geophys., Extended Abstracts, No. G051.

Rommel, B. E., 1993b, Stacking Velocity of Converted Waves in Weakly Transversely Isotropic Layers: 55th Mtg., Europ. Assn. Expl. Geophys., Extended Abstracts, No. P128.

Rommel, B. E., 1993a, Approximate Stacking Velocitities in a Weakly Transversely Isotropic Layer: Can. J. Expl. Geophys., **29**, 98–105.

Sheriff, R. E., and Geldart, L. P., 1982. Exploration seismology, Vol. 1: History, theory and acquisition: Cambridge Univ. Press.

Tessmer, G., and Behle, A., 1988, Common reflection point data-stacking technique for converted waves: Geophys. Prosp., **36**, 671-688.

Thomsen, L., 1986, Weak elastic anisotropy: Geophysics, **51**, 1954-1966.

APPENDIX A: Asymptote of the Reflection Point

For a mode-converted wave the reflection point, even on a horizontal reflector, is not located directly beneath the midpoint, but depends on the elastic properties and the reflector depth. For small offset-to-depth ratios, however, the reflection point approaches an asymptote. Here, I calculate this asymptote, also taking reflector dip into account.

First, I derive a relationship between the reflector depth and the shot-receiver distance. Second, I derive a relationship between the reflection point and the reflector depth. Combining both I establish a relationship between the reflection point and the shot-receiver distance. This final relationship depends only on the reflector dip and the ray angles. The ray angle of the upgoing wave can be expressed in terms of the ray angle of the downgoing wave and the reflector dip.

A.1 Geometry of the raypath

In the following, I use the notation of Figure A.1. A ray travels down from the source point S to the reflection point D, which will be common to all rays of a CRP gather, and from the reflection point D up to the receiver G. The reflector normal through the reflection point D intersects the surface at point N. This point differs from the intersection point O of the zero-offset ray with the surface, since, in an anisotropic medium, the zero-offset ray is generally not normal to the reflector. Nevertheless, it is more convenient to define the ray angles ϕ_S, ϕ_R of the downgoing and upgoing wave, respectively, relative to the reflector normal, not relative to the vertical or to the zero-offset ray. Also, I use the coordinates x_S, x_R for the location of the source S and the receiver R, respectively.

The length l_S of the raypath from the source S to the reflection point R in terms of the reflector depth d_S, dip φ and ray angle ϕ_S of the downgoing wave is

$$l_S = \frac{d_S}{\cos\phi_S}. \tag{A.1}$$

Accordingly, the length l_R of the raypath from the reflection point D to the receiver R is

$$l_R = \frac{[d_S + (x_R - x_S)\sin\varphi]}{\cos\phi_R}, \tag{A.2}$$

where x denotes the source-receiver distance $x_R - x_S$.

Define an auxiliary line running parallel to the reflector from the reflector normal to the source S. Its length l_A is

$$\begin{aligned} l_A &= l_S \sin\phi_S \\ &= d_S \tan\phi_S. \end{aligned} \tag{A.3}$$

The distance $x_S - x_N$ between the source S and the surface point N can now be expressed in terms of the reflector depth d_S, dip φ and ray angle ϕ_S of the downgoing wave:

$$x_N - x_S = \frac{l_A}{\cos\varphi} \tag{A.4}$$

$$= \frac{d_S \tan\phi_S}{\cos\varphi}. \tag{A.5}$$

Accordingly, the distance $x_R - x_N$ between the surface point N and receiver point R is

$$x_R - x_N = \frac{[d_S + (x_R - x_S)\sin\varphi]\tan\phi_R}{\cos\varphi}. \tag{A.6}$$

The total shot-receiver distance is, of course, the sum of both. Rearranging this sum, I obtain the reflector depth d_S in terms of the shot-receiver distance $x_R - x_S$:

$$d_S = \frac{\cos\varphi - \sin\varphi\tan\phi_R}{\tan\phi_S + \tan\phi_R}(x_R - x_S). \tag{A.7}$$

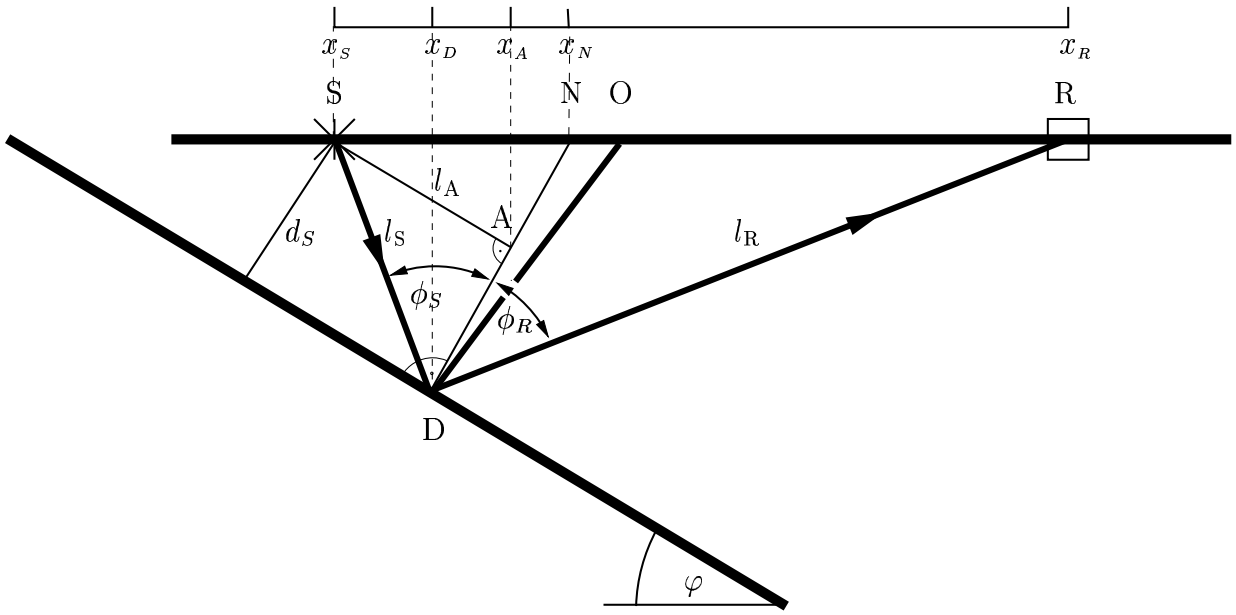

Figure A.1. Notation: The following points are used: source S, reflection D, zero-offset 0, and receiver R. The coordinate x_S denotes the horizontal location of the source S, x_D that of the reflection point D, x_A that of the auxiliary point A, and x_R that of the receiver R. Distance d_S is measured parallel to the normal to the reflector through the source point S. Distances l_S and l_G are measured from the source point S to the reflection point D, and from the reflection point D to the receiver point R, respectively. The thin line from the reflection point D to the surface is the reflector normal, and the thick line represents a potential zero-offset ray. Distance l_A is measured parallel to the reflector from the source S to the auxiliary point A on the reflector normal. The ray angles $\phi_S = \sphericalangle(\text{NDS})$ and $\phi_R = \sphericalangle(\text{NDR})$ are measured with respect to the reflector normal; each ray angle corresponds to a phase angle (not shown here). The reflector dip φ is measured with respect to the horizontal.

This is the first relationship, the one between the reflector depth and the source-receiver distance, as mentioned above.

Now, define the intersection point A of the auxiliary line and the reflector normal. The horizontal distance $x_A - x_S$ from the shotpoint S to the intersection point A is $l_A \cos\varphi$. It is larger than the horizontal distance $x_D - x_S$ of the reflection point D by $d_S \sin\varphi$. Hence, the horizontal distance $x_D - x_S$ from the source S to the reflection point D is

$$x_D - x_S = l_A \cos\varphi - d_S \sin\varphi \qquad \text{(A.8)}$$

$$= d_S \left(\tan\phi_S \cos\varphi - \sin\varphi\right). \qquad \text{(A.9)}$$

This is the second relationship, the one between the reflector depth and the horizontal distance of the reflection point, as described above.

Now, I insert the reflector depth (A.7) into the expression (A.8) for $x_D - x_S$:

$$x_D - x_S = \frac{\cos\varphi - \sin\varphi \tan\phi_G}{\tan\phi_S + \tan\phi_G} \cdot \left(\tan\phi_G \cos\varphi - \sin\varphi\right)\left(x_R - x_S\right). \qquad \text{(A.10)}$$

For an anisotropic medium, the dependence of the ray angles on the elastic properties and the reflector dip φ is complicated. Therefore, I restrict the analysis to the limit of a small offset-to-depth ratio. In this limit, the rays approach the zero-offset ray. However, for an anisotropic medium, the zero-offset ray does not generally coincide with the reflector normal; consequently, the ray angles that are defined relative to the reflector normal, do not generally vanish. In the weak-anisotropy approximation, the deviation between the zero-offset ray and reflector normal is considered small. Hence, I can approximate the tangent in terms of the sine, $\tan\phi \approx \sin\phi$ and $\sin\phi \gg \sin^2\phi$, choosing the sine to later apply Snell's law. With this assumption of small ray angles, the horizontal reflection distance x_D (A.10) becomes

$$x_D - x_S = \frac{\sin\phi_R - \sin\varphi\cos\varphi}{\sin\phi_S + \sin\phi_R}\left(x_R - x_S\right). \qquad \text{(A.11)}$$

This, of course, includes the known case of a horizontal reflector (with $\varphi \equiv 0°$) and an isotropic layer, where phase and ray angles are equal, and Snell's law reads $\sin\theta_p = v_p/v_s \sin\theta_s$. Specializing the approximate horizontal distance x_D (A.11) for a *P-SV* wave in an isotropic medium yields

$$x_D - x_S = \frac{1}{1 + \frac{v_S}{v_P}}\left(x_R - x_S\right). \qquad \text{(A.12)}$$

which matches Tessmer and Behle's (1988) result.

A.2 Approximate ray angles

The reflection distance x_D (A.11) contains the ray angles ϕ_S, ϕ_R of the downgoing and upgoing wave. Of course, these ray angles are not independent of each other. The ray angles are indirectly linked together by Snell's law; to be precise, the ray angles are linked to their corresponding phase angles, and Snell's law works on the phase angles. The exact relationship between the ray angles is not an algebraic function of the sine. Hence, I approximate this relationship in terms of Thomsen's (1986) anisotropy coefficients.

For now, I define the angles with respect to the symmetry axis, not the reflector normal. Then, for small anisotropy coefficients δ and ϵ the relationship between the ray angle ϕ and phase angle θ of the P-wave is approximately (Rommel, 1993b)

$$\phi_p \approx \theta_p + 2\delta \sin\theta_p + 2\,(\epsilon-\delta)\sin^3\theta_p. \tag{A.13}$$

The corresponding relationship for the SV-wave is

$$\phi_s \approx \theta_s + 2\frac{{v_{p0}}^2}{{v_{s0}}^2}\,(\epsilon-\delta)\sin\theta_s + 2\frac{{v_{p0}}^2}{{v_{s0}}^2}\,(\epsilon-\delta)\sin^3\theta_s, \tag{A.14}$$

where v_{p0} and v_{s0} denote the phase velocities of the P-wave and SV-wave, respectively, in the vertical direction. However, I need the sine of the ray angle ϕ_s [see equation (A.11)],

$$\sin\phi_s \approx \left[1 + 2\frac{{v_{p0}}^2}{{v_{s0}}^2}\,(\epsilon-\delta)\cos\theta_s + 4\frac{{v_{p0}}^2}{{v_{s0}}^2}\,(\epsilon-\delta)\cos\theta_s\sin^2\theta_s\right]\cdot \sin\theta_s. \tag{A.15}$$

To express the SV-ray angle ϕ_s in terms of the P-ray angle ϕ_S, I apply Snell's law. This replaces $\sin\theta_s$ by $[v_s(\theta_s)/v_p](\theta_p)\sin\theta_p$. However, the phase velocities themselves also depend on the phase angles. Thomsen's (1986) approximation of the SV-phase velocity reads

$$v_s(\theta_s) \approx v_{s0}\cdot \left[1 + 2\frac{{v_{p0}}^2}{{v_{s0}}^2}\,(\epsilon-\delta)\sin^2\theta_s - 2\frac{{v_{p0}}^2}{{v_{s0}}^2}\,(\epsilon-\delta)\sin^4\theta_s\right]. \tag{A.16}$$

On the right side, $\sin\theta_s$ is replaced repeatedly by $[v_s(\theta_s)/v_p](\theta_p)\sin\theta_p$. The iteration, however, stops if we consider only a finite order of anisotropy coefficients. Approximating the right side to the first order of the anisotropy coefficients gives

$$v_s(\theta_s) \approx v_{s0}\cdot \left[1 + 2\,(\epsilon-\delta)\sin^2\theta_p - 2\frac{{v_{s0}}^2}{{v_{p0}}^2}\,(\epsilon-\delta)\sin^4\theta_p\right]. \tag{A.17}$$

Now, let us express the SV-phase velocity in terms of the P-phase angle. Recall that Thomsen's (1986) approximation of the P-phase velocity reads

$$v_p(\theta_p) = v_{p0}\cdot \left[1 + 2\delta\sin^2\theta_p + 2\,(\epsilon-\delta)\sin^4\theta_p\right]. \tag{A.18}$$

Using these phase velocities (A.17 and A.18), Snell's law for a weakly anisotropic medium becomes

$$\sin\theta_s \approx \frac{v_{s0}}{v_{p0}}\cdot \left\{1 + 2\,(\epsilon-2\delta)\sin^2\theta_p - 2\left(\frac{{v_{s0}}^2}{{v_{p0}}^2}-1\right)(\epsilon-\delta)\sin^4\theta_p\right\}. \tag{A.19}$$

Now, use Snell's law to replace SV-phase angle θ_s in the expression of the SV-ray angle (A.15). Unfortunately, this expression also contains the cosine of the SV-phase angle; hence, the resulting equation is not algebraic. Therefore, let us consider the simplest case only, that of a dipping reflector with a symmetry axis perpendicular to the reflector. In this case, the ray angles ϕ_p and ϕ_s become small because, in the limit, the zero-offset ray approaches the symmetry axis. With this assumption,

Snell's law reads

$$\sin\phi_s \quad = \quad \frac{v_{s0}}{v_{p0}}\left[1+2\frac{{v_{p0}}^2}{{v_{s0}}^2}(\epsilon-\delta)\right]\sin\theta_p. \qquad \text{(A.20)}$$

In the same approximation for weak anisotropy and small angles, the P-ray angle becomes

$$\sin\phi_p \quad \approx \quad [1+2\delta]\sin\theta_p. \qquad \text{(A.21)}$$

A.3 Reflection distance for a converted wave

A.3.1 Dipping reflector

Assume that the symmetry axis is perpendicular to the reflector. Therefore, the ray angles vanish in the limit of a small offset-to-depth ratio (see Figure A.1), regardless of the actual reflector dip.

Here, let us consider a P-to-SV mode-converted wave, that is a P-wave on the source side and a SV-wave on the receiver side. Above, we obtained the relationship between the P- (A.21) and the SV-ray angles (A.20) in terms of the P-phase angle. Inserting these wave-specific properties are inserted into the reflection distance (A.11) gives

$$\begin{aligned} & x_D - x_S \\ \approx \quad & \frac{\sin\phi_p - \sin\varphi\cos\varphi}{\sin\theta_p\left\{1+2\delta+\frac{v_{s0}}{v_{p0}}\left[1+2\frac{{v_{p0}}^2}{{v_{s0}}^2}(\epsilon-\delta)\right]\right\}}\cdot \\ & (x_R - x_S)\,. \end{aligned} \qquad \text{(A.22)}$$

Replacing the P-phase angle θ_p by the observable P-ray angle, $\sin\phi_p = \sin\theta_p\,[1+2\delta]$ (A.21), gives

$$\begin{aligned} & x_D - x_S \\ \approx \quad & \frac{1-\frac{\sin\varphi\cos\varphi}{\sin\phi_p}}{1+\frac{v_{s0}}{v_{p0}}\frac{\left[1+2\frac{{v_{p0}}^2}{{v_{s0}}^2}(\epsilon-\delta)\right]}{[1+2\delta]}}(x_R - x_S)\,. \end{aligned} \qquad \text{(A.23)}$$

In the limit of infinite reflector depth the ray angle ϕ_p vanishes and, thus,

$$\begin{aligned} & x_D - x_S \\ \to \quad & -\frac{\sin\varphi\cos\varphi}{1+\frac{v_{s0}}{v_{p0}}\frac{\left[1+2\frac{{v_{p0}}^2}{{v_{s0}}^2}(\epsilon-\delta)\right]}{[1+2\delta]}}\frac{x_R - x_S}{\sin\phi_p}. \end{aligned} \qquad \text{(A.24)}$$

is the dominating term. As the ray angle ϕ_p approaches 0, the right side goes to negative infinity. In fact, $\sin\phi_p = l_A/l_S \approx l_A/d_S$ (A.3) becomes proportional to the inverse of the reflector depth. Since all other factors are constant, the reflection distance $x_D - x_S$ decreases linearly with depth. The asymptote is no longer vertical, but inclined.

A.3.2 Horizontal reflector

Only for a horizontal reflector, where $\varphi \equiv 0°$, is the reflection distance $x_D - x_S$ (A.24) not defined. For this case, I specialize the general expression of reflection distance $x_D - x_S$ (A.10), yielding

$$\begin{aligned} & x_D - x_S \\ = \quad & \frac{\tan\phi_R}{\tan\phi_S+\tan\phi_R}(x_R - x_S)\,. \end{aligned} \qquad \text{(A.25)}$$

Again, consider a P-to-SV mode-converted wave. In an analogous manner (as in A.2), we can expand the tangent in terms of the sine and insert the expressions of the ray angles ϕ_p (A.21), ϕ_s (A.20). Now, the leading term is constant (Rommel, 1995a):

$$\begin{aligned} & x_D - x_S \\ \to \quad & \frac{1}{1+\frac{v_{s0}}{v_{p0}}\frac{\left[1+2\frac{{v_{p0}}^2}{{v_{s0}}^2}(\epsilon-\delta)\right]}{[1+2\delta]}}(x_R - x_S)\,. \end{aligned} \qquad \text{(A.26)}$$